A LETTERS JOURNAL EXPLORING THE FRONTIERS OF PHYSICS

OFFPRINT

A scaling law for heat conductivity in sheared granular materials

P. ROGNON, I. EINAV, J. BONIVIN and T. MILLER

EPL, **89** (2010) 58006

A Letters Journal Exploring the Frontiers of Physics

March 2010

EPL, **89** (2010) 58006 www.epljournal.org
doi: 10.1209/0295-5075/89/58006

A scaling law for heat conductivity in sheared granular materials

P. Rognon[(a)], I. Einav, J. Bonivin and T. Miller

School of Civil Engineering, J05, The University of Sydney - Sydney, New South Wales 2006, Australia

received 13 January 2010; accepted in final form 23 February 2010
published online 30 March 2010

PACS 81.05.Rm – Porous materials; granular materials
PACS 65.20.-w – Thermal properties of liquids
PACS 91.30.Ab – Theory and modeling, computational seismology

Abstract – We investigate the heat transfer through the contact network of a sheared granular material using the standard Discrete Element Method. Elastic and frictional grains are subjected to steady and uniform plane shear. The effective conductivity tensor is expressed through the sum of contact conductances, which enables instantaneous measurements without simulating the actual heat transfer. We show that the conductivity i) does not depend on the *inertial number* I which controls the shear state, ii) increases with grain deformations (higher confining stress or lower Young's modulus) and iii) decreases for higher friction coefficients. We extract a robust semi-empirical scaling which quantitatively relates the conductivity to the contact density, Young's modulus and the part of the stresses that carries only the normal forces.

Introduction. – Heat transfer through granular materials is a long-standing problem broadly involved in industrial processes, in civil engineering and in geophysical events. Perhaps the most salient issue relates to the coupling between the mechanical properties of the material and its temperature. For instance, the heat treatment of clayey soil at temperatures beyond roughly 100 °C results in hardening, a decrease of the plastic limit and an enhanced resistance against disintegration when soaked in water. This has been empirically well known for about 20000 years —since the use of pottery [1]. More recently, various numerical and experimental studies focused on the thermal expansion of grains, and showed it to be the leading mechanism for granular compaction during thermal cycling [2–5]. Controlling the heat treatment of clayed soils and the thermal granular compaction requires an accurate understanding of how the heat flows through static granular samples. This has been investigated in previous works (see for instance [6–10]).

In geophysics, the shear heating of brittle rocks in fault gouges during earthquakes is a *hotly* debated question [11–13]. The rising temperature within the fault is pivotal to its behaviour. It leads to a pressurization of the pore fluide, which can induce the fluidization of the material [13–15]. In siliceous materials, rising temperatures could even lead to grain melting [16]. In sheared granular layers, temperature rise can occur even without external heating, as a result of heat production from the dissipation of mechanical energy [17], and the relative inability of the layer to transfer this heat outside. This heat transfer involves various complex mechanisms: the conduction through the contact network, the conduction and convection through the fluid, and the radiation between grain surfaces [6,7]. These mechanisms are likely a function of the characteristics of the shear, though to our knowledge such relationships have not been established yet.

In this letter we focus on the heat conduction through the contact network within sheared granular layers. We use a standard Discrete Element Method (DEM) to simulate the dynamics of elastic and frictional spheres subjected to plane shear. We express the effective conductivity tensor through the sum of the thermal conductance between pairs of contacting grains. This expression enables direct and instantaneous measurements of conductivity during the shear without having to simulate the actual heat transfer. It is then being used to investigate the scaling of the material thermal conductivity as a function of the imposed stresses and shear strain rates, in relation to the grain stiffnesses and friction coefficients.

At the contact level. – The contact between two grains transmits forces and conducts heat. Let us recall the usual models that describe these two processes in isolation, for spherical elastic frictional grains of diameter d, mass m, Young's modulus E, friction coefficient μ and conductivity k_s. For both the mechanical and thermal

[(a)] E-mail: prognon@usyd.edu.au

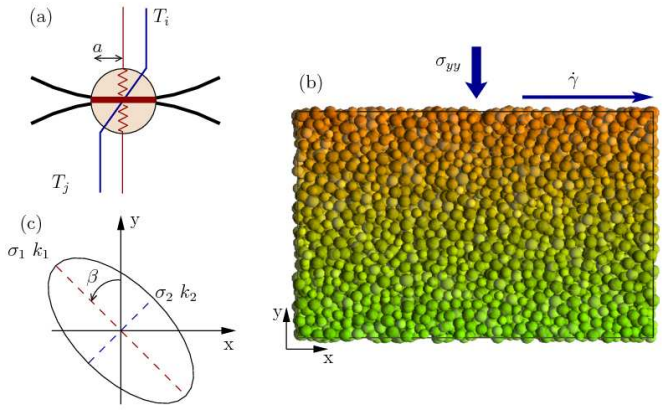

Fig. 1: (Color online) Thermal conduction in plane shear flow, DEM simulations. (a) Contact between two elastic grains with different temperatures; both the elastic energy (red springs) and temperature gradient (blue line) are mostly contained in the small region of size a represented by the filled circles (see eq. (1)). (b) Plane shear flow of 5000 spheres in a three-dimensional periodic domain; the nominal shear strain rate $\dot{\gamma}$ is prescribed and the normal stress σ_{yy} is kept constant by dilating and contracting the cell during the shear. (c) Representation of the stress tensor $\boldsymbol{\sigma}$ and the effective conductivity tensor $\boldsymbol{k}$ by an ellipse to illustrate the meaning of the eigenvalues (subscripts 1 and 2) and the angle β.

problems, consider a perfect contact between smooth surfaces with no asperities (fig. 1(a)).

Hertz's theory relates the normal force F_n that the grain surface experiences at the contact point to the normal deflection δ_n [18]. As long as the deflection is much smaller than the grain size ($\delta_n \ll d$), the contact area is a disk whose radius a depends on the normal deflection:

$$a \approx \sqrt{d\delta_n}. \tag{1}$$

We will refer to a as the contact size from here on. Although the surface deflection induces some elastic strain within the whole grain, most of the elastic energy is being stored in a small region of size a near the contact point. Within this region, the elastic strain scales with δ_n/a, so that the elastic energy ξ_n scales with $Ea^3(\frac{\delta_n}{a})^2$. The corresponding normal force is the derivative of this energy with respect to the deflection δ_n. Using eq. (1) leads to

$$F_n = \alpha_n E d^{\frac{1}{2}} \delta_n^{\frac{3}{2}} = \alpha_n E a \delta_n = \alpha_n E \frac{a^3}{d}, \tag{2}$$

where α_n is a numerical constant of the order of unity. The relation between the tangential force F_t and the tangential deflection δ_t can be expressed using a similar approach. Considering that the elastic strain induced by the tangential deflection is mostly contained in a small region of size a near the contact point where it scales with δ_t/a, the corresponding elastic energy ξ_t scales with $Ea^3(\frac{\delta_t}{a})^2$. The tangential force is the derivative of this energy with respect to the tangential deflection δ_t. Using eq. (1) leads to

$$F_t = \alpha_t E a \delta_t, \tag{3}$$

where α_t is a numerical constant of the order of unity. For Coulomb's friction, this tangential force is limited by the sliding of the surfaces: there is no sliding if $F_t < \mu F_n$, but $F_t = \mu F_n$ when sliding occurs.

The heat conduction through a narrow contact of size a is a complex problem when the surfaces are rough [19,20]. For perfectly smooth surfaces, a simple model relates the heat flux ϕ_{ij} from grain i to grain j to the temperatures T_i and T_j at their centers [21–23]. Due to the constriction of the heat flux at the narrow contact, most of the temperature gradient is contained within a region of typical size a near the contact, while the temperature outside this region is almost homogeneous. The temperature gradient near the contact scales with $(T_j - T_i)/(2a)$, and the heat flux from particle i to particle j is then

$$\phi_{ij} = -2ak_s(T_j - T_i). \tag{4}$$

The main outcomes of this thermo-mechanical analysis at the contact level is that the heat flux between two grains is proportional to the contact size a, and that the contact size depends only on the normal contact force F_n: $a \propto F_n^{\frac{1}{3}}$; in other words it is independent of the tangential force.

Summing the contact contributions. – It is useful to note that both the elastic strain and the temperature gradient are contained mostly within a small region of size a adjacent to the contact. For small contacts ($a \ll d$), this ensures that several contacts on a single grain would not interact with each other, either mechanically or thermally. Consequently, the contacts are independent and their effects can be summed up to build the effective thermo-mechanical properties of the sample. The stress tensor $\boldsymbol{\sigma}$ is thus often built as [24,25]

$$\boldsymbol{\sigma} = \frac{1}{V} \sum_c \vec{F}^c \otimes \vec{r}^{\,c}, \tag{5}$$

where V is the volume of the sample, $\vec{F}^c$ is the force at the contact c, $\vec{r}^{\,c}$ is the center-to-center vector of the two particles involved, and the sum runs over every contact.

Thanks to the thermal independence of the contacts, the tensor of effective conductivity $\boldsymbol{k}^{eff}$ can also be derived as a sum of contact heat fluxes. According to Fourier's law, when the material experiences an homogeneous temperature gradient $\vec{\nabla}T$, the effective heat flux density $\vec{q}$ is

$$\vec{q} = -\boldsymbol{k}^{eff} \cdot \vec{\nabla}T. \tag{6}$$

Considering that each contact transfers heat from the center of a particle to the center of another with a flux ϕ_c, the total heat flux density can be expressed as a sum of heat flux at every contact:

$$\vec{q} = \frac{1}{V} \sum_c \phi^c \vec{r}^{\,c}. \tag{7}$$

Using eq. (4) and considering that the temperature difference between two contacting particles relies on the temperature gradient as $T_j - T_i = \vec{r}^{\,c} \cdot \vec{\nabla} T$, the heat flux density can be expressed as $\vec{q} = -2k_s/V \sum_c a^c \vec{r}^{\,c} \otimes \vec{r}^{\,c} \cdot \vec{\nabla} T$. The tensor of effective conductivity is then identified as

$$\boldsymbol{k}^{eff} = \frac{2k_s}{V} \sum_c a^c \vec{r}^{\,c} \otimes \vec{r}^{\,c}. \tag{8}$$

This formulation of effective conductivity is consistent with the derivation introduced in [26], which involves the continuous distribution of contact orientation and that of the contact size rather than a discrete sum of the contact contributions. It enables instantaneous measurements of the effective conductivity tensor without having to simulate the actual heat transfer in the material. Deducing the conductivity from the measurements of heat flux and temperature gradients could be done using the thermal-DEM, as introduced in [8,9], though it would require more complex procedures such as the hot-strip method [27].

Steady and uniform plane shear. – The DEM material consists of 5000 spheres interacting with frictional and elastic contacts as well as rolling resistance and twist friction. We use eqs. (2) and (3) for the elastic forces, with constants $\alpha_{n,t} = 1$. The twist and rolling moments $\Gamma^{t,r}$ depend on the twist and rolling angles $\psi^{t,r}$: $\Gamma^{t,r} = Ea^3\psi^{t,r}$ (see [28]). There is no twist sliding as long as $\Gamma^t < \frac{8}{15}\mu a F^n$ and no rolling as long as $\Gamma^r < aF^n$.

The sample experiences a plane shear loading with a prescribed normal stress σ_{yy} and a prescribed shear strain rate $\dot{\gamma}$. The loading is applied through periodic boundaries to eliminate the wall effects as much as possible (see fig. 1(b)). There is no gravity, and since no localisation develops the stresses are homogeneous across the sample.

The initial configuration is usually a static sample undergoing a confining normal stress σ_{yy}. The sample is then sheared until a nominal shear strain γ of 10 is reached. There is a first transient lasting few γ during which the sample dilates and the coordination number decreases (see fig. 2). Then the material reaches a steady state with some fluctuations about the mean values of stresses, kinetic energy, coordination number Z and volume fraction ν (ratio of the volume of the grains to the total volume). We check that this final steady state does not depend on the initial volume fraction and velocity profile, as in [29,30]. The measurements are averaged over time within the steady state on a set of about 50 snapshots taken every 0.1γ.

The physical quantities will be expressed in the natural set of units related to the grains: their mass m, their size d, their bulk conductivity k_s and their Young's modulus E. The plane shear loading is controlled through two dimensionless numbers: the stiffness number $\kappa = \frac{\sigma_{yy}}{E}$ and the inertial number $I = \dot{\gamma}\sqrt{\frac{m}{d\sigma_{yy}}}$ [29,31,32]. The range of parameters investigated is given in table 1.

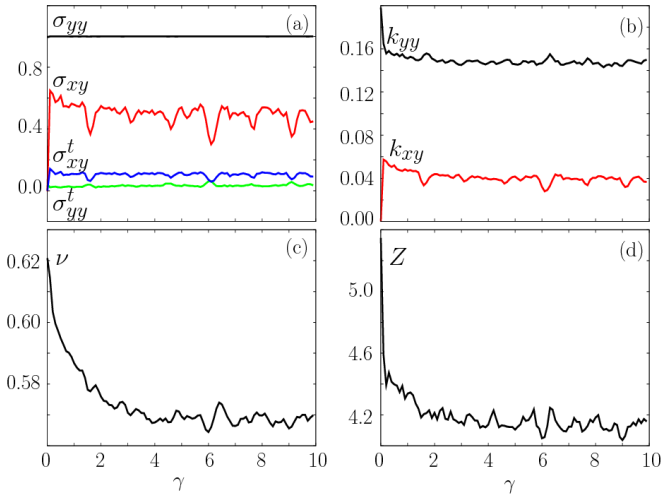

Fig. 2: (Color online) Arriving at the steady shear state ($I = 0.01$, $\kappa = 10^{-3}$ and $\mu = 0.4$), with increasing shear strain γ: (a) the normal (positive in compression) and shear components of the stress tensor (σ_{yy} and σ_{xy}) and the part of these stresses that carries only the tangential contact forces (σ^t_{yy} and σ^t_{xy}); (b) the normal and shear (absolute value) conductivities (k_{yy} and k_{xy}); (c) the solid fraction ν; (d) the coordination number Z. In this example, the steady state is reached when γ is bigger than roughly 4.

Table 1: Range of dimensionless parameters investigated: the inter-granular friction coefficient μ, the stiffness number κ and the inertial number I. This set roughly corresponds to the shear of a one kilometer deep fault gauge ($\sigma_{yy} \approx 10^7$ Pa) with grains of Young's modulus $E \approx 10^{10}$ Pa and diameter $d \approx 10^{-3}$ m (mass $m \approx 10^{-6}$ kg), for shear strain rates ranging between $3.10^2\,\mathrm{s}^{-1}$ and $10^4\,\mathrm{s}^{-1}$.

μ	$\kappa = \frac{\sigma_{yy}}{E}$	$I = \dot{\gamma}\sqrt{\frac{m}{d\sigma_{yy}}}$
$0 \to 0.8$	$3 \cdot 10^{-4} \to 3 \cdot 10^{-3}$	$3 \cdot 10^{-3} \to 10^{-1}$

Conductivity *vs.* stresses. – Both the conductivity and the stress are symmetric tensors according to their construction followed in this paper. They are characterised by three eigenvalues and only one angle β due to the transverse symmetry induced by the plane shear flow (see fig. 1(c)). For every system under consideration, we observe that the angle β is about 45°, with fluctuations lower than 1°. They are thus characterised by their two eigenvalues in the major and minor compression directions, $\beta = 45°$ and $\beta = -45°$, which we refer to with subscripts 1 and 2, respectively. Figure 3 shows the evolution of the eigenconductivities k_1 and k_2, and that of the eigenstresses σ_1 and σ_2 (positive in compression) as a function of the inter-granular friction μ, the rigidity κ and the inertial number I. Both eigenconductivities reach a maximum for a low value of friction and significantly decrease as the friction increases. The eigenconductivities also strongly increase as grains get more deformed, and are mostly independent of the inertial number. The

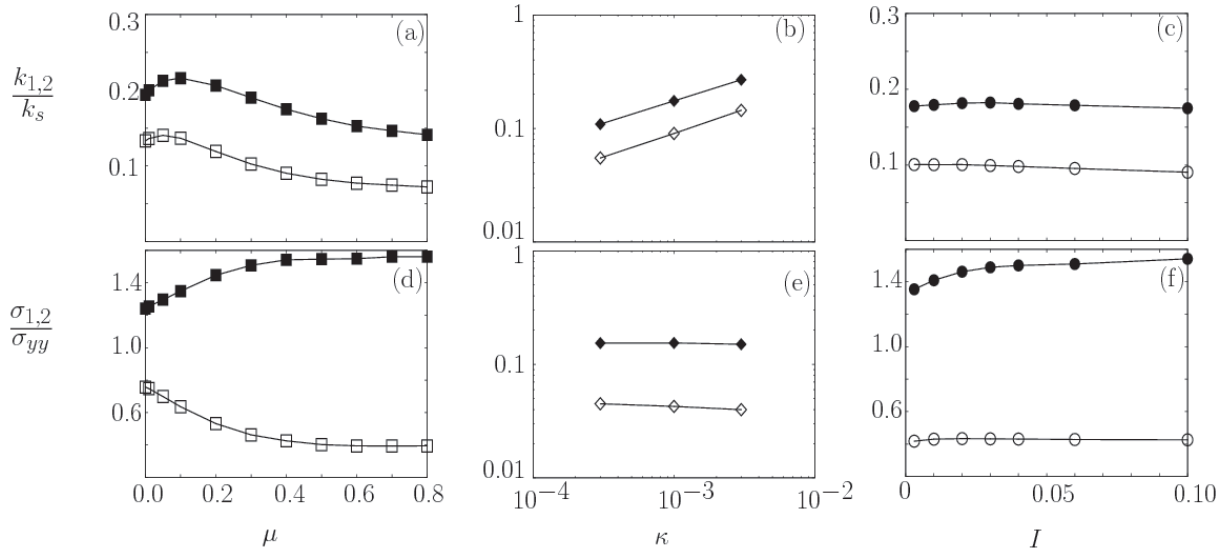

Fig. 3: Eigenconductivities k_1 and k_2 (upper plots) and eigenstresses σ_1 and σ_2 (lower plots) as a function of: (a), (d) the inter-granular friction coefficient μ ($I = 0.1$, $\kappa = 10^{-3}$); (b), (e) the stiffness number κ ($\mu = 0.4$, $I = 0.1$); (c), (f) the inertial number I ($\mu = 0.4$, $\kappa = 10^{-3}$). Filled symbols denote the major eigenvalues (subscript 1, high-compression direction) and open symbols denote the minor eigenvalues (subscript 2, low-compression direction).

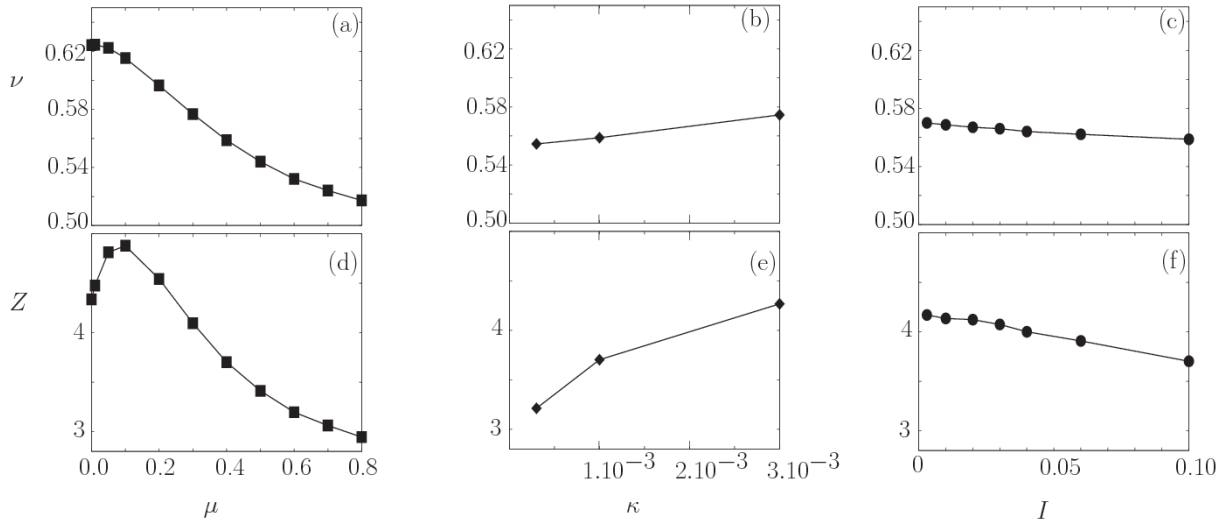

Fig. 4: Solid fraction ν (upper plots) and coordination number Z (lower plots) as a function of: (a), (d) the inter-granular friction coefficient μ ($I = 0.1$, $\kappa = 10^{-3}$); (b), (e) the stiffness number κ ($\mu = 0.4$, $I = 0.1$); (c), (f) the inertial number I ($\mu = 0.4$, $\kappa = 10^{-3}$).

comparison of the evolution of the eigenconductivities and the eigenstresses clearly indicates that there is no direct or unique relationship between them.

Scaling. – The missing components of such a scaling can be deduced from the expressions of the stress and conductivity tensors in eqs. (5) and (8). Both the stress and the conductivity tensors involve the sum over all the contacts divided by the volume of the cell. They are therefore intrinsically dependent on the contact density, which can be expressed as the coordination number Z times the solid fraction ν (ratio of the volume of the grains to the volume of the cell). Figure 4 shows the evolution of these two quantities with respect to the friction coefficient μ, the stiffness number κ and the inertial number I. According to previous studies, the dilatancy as well as a decrease in the coordination number are induced either by increasing the inertial number [29–32], or increasing the grain rigidity [33]. The dilatancy is strongly enhanced by friction, while the coordination reaches a maximum of about 6 for a low value of friction and then decreases for higher values. These values are compatible with the theoretical value of isostaticity reported in previous studies (see for instance the discussion in [34]), but this field is still largely open for dynamics systems of soft grains as ours.

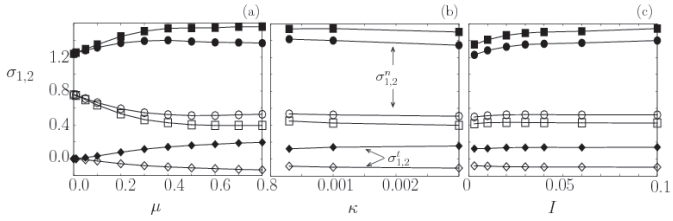

Fig. 5: Decomposition of the total stresses $\boldsymbol{\sigma}$ (■) into two components due to either the normal forces $\boldsymbol{\sigma}^n$ (●) or the tangential forces $\boldsymbol{\sigma}^t$ (♦), as a function of: (a) the inter-granular friction coefficient μ ($I = 0.1$, $\kappa = 10^{-3}$); (b) the stiffness number κ ($\mu = 0.4$, $I = 0.1$); (c) the inertial number I ($\mu = 0.4$, $\kappa = 10^{-3}$). Filled symbols denote the major eigenvalues (subscript 1, high-compression direction) and open symbols denote the minor eigenvalues (subscript 2, low-compression direction).

The stress tensor can be expressed as the sum of two components: the stresses due to the normal forces, $\boldsymbol{\sigma}^n$, and the stresses due to the tangential forces, $\boldsymbol{\sigma}^t$:

$$\boldsymbol{\sigma} = \boldsymbol{\sigma}^n + \boldsymbol{\sigma}^t = \frac{1}{V} \sum_c \left(\vec{F}^c_n + \vec{F}^c_t \right) \otimes \vec{r}^{\,c}. \tag{9}$$

The conductivity tensor involves the contact size a which depends only on the normal force. It is thus independent of the part of the stresses that carries the tangential forces, $\boldsymbol{\sigma}^t$, while a scaling with $\boldsymbol{\sigma}^n$ is expected. In static compression, the component of the stresses due to the tangential forces is low, around few percent of the total stresses [35]. Therefore, there is a little difference between the total stresses and the stresses due to the normal forces. Figure 5 shows the contribution of the normal and tangential forces to the eigenstresses as a function of the various parameters. In plane shear, unlike in static compression, the tangential forces contribute significantly to the total stresses, approximately up to 20%.

Let us now express the conductivity tensor and the part of the stress tensor due to the normal forces in term of the contact density $Z\nu$:

$$\boldsymbol{k}^{eff} = 2k_s \nu Z d^2 \langle a \boldsymbol{r} \rangle \tag{10}$$

$$\boldsymbol{\sigma}^n = E \nu Z \langle a^3 \boldsymbol{r} \rangle \tag{11}$$

$\langle \cdot \rangle$ denotes an average over all the contacts, and we use $\boldsymbol{r} = d^{-2} \vec{r} \otimes \vec{r}$. We combine these two equations to get

$$\boldsymbol{k}^{eff} = 2k_s \left(\nu Z d^3 \right)^{\frac{2}{3}} \left(\frac{\boldsymbol{\sigma}^n}{E} \right)^{\frac{1}{3}} \langle a \boldsymbol{r} \rangle \langle a^3 \boldsymbol{r} \rangle^{-\frac{1}{3}}. \tag{12}$$

Therefore, for a material with an isotropic stress σ_{yy} and an isotropic conductivity k^{eff}_{yy} (both $\langle a \boldsymbol{r} \rangle$ and $\langle a^3 \boldsymbol{r} \rangle$ are then isotropic) we expect the following scaling:

$$k^{eff}_{yy} = 2k_s \left(\nu Z d^3 \right)^{\frac{2}{3}} \kappa^{\frac{1}{3}}. \tag{13}$$

This scaling obviously ignores the anisotropy of stress and conductivity tensors as induced by the plane shear. In

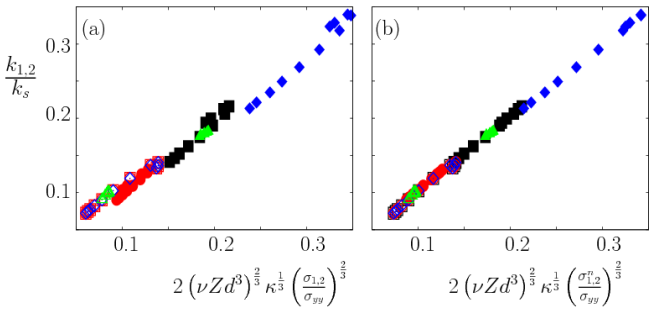

Fig. 6: (Color online) Scaling of the eigenconductivities as a function of the eigenstresses, the coordination number Z and the solid fraction ν as proposed in eq. (14): (a) including the total stress $\boldsymbol{\sigma}$; (b) including the stresses supported only by the normal forces, $\boldsymbol{\sigma}^n$. Filled symbols denote the major eigenvalues (subscript 1, high-compression direction) and open symbols denote the minor eigenvalues(subscript 2, low-compression direction). The results from all the simulations collapse along a single line: three series with $I = 0.1$, μ ranging between 0 and 0.8, and $\kappa = 3 \cdot 10^{-4}$ (●), $\kappa = 10^{-3}$ (■), $\kappa = 3 \cdot 10^{-3}$ (♦); one series with $\mu = 0.4$, $\kappa = 10^{-3}$ and I ranging from $3 \cdot 10^{-3}$ to 10^{-1} (▲).

order to consider these anisotropy effects, let us investigate a scaling law in the following form:

$$k^{eff}_{1,2} = 2k_s \left(\nu Z d^3 \right)^{\frac{2}{3}} \kappa^{\frac{1}{3}} \left(\frac{\sigma^n_{1,2}}{\sigma_{yy}} \right)^b. \tag{14}$$

As the tangential forces contribute less than 3% to the normal stress, it is possible to assert that $\sigma_{yy} \approx \sigma^n_{yy}$ (see fig. 2). Then $\kappa = \sigma_{yy}/E$ accounts for the average contact size. $(\frac{\boldsymbol{\sigma}^n}{\sigma_{yy}})^b$ accounts for the anisotropy of the normal force distribution. Without any apparent theoretical support, the above equation fits quite remarkably all the conductivity values obtained for various friction coefficients μ, stiffness numbers κ and inertial numbers I, using the power coefficient of $b = 2/3$ (see fig. 6). The success of the anisotropic form of the scaling is highlighted against the isotropic one obtained when considering the total stress instead of the stress due to normal forces.

Conclusion. – This paper focused on the conduction problem through the contact network of sheared granular materials. Using a standard DEM, we investigated steady and uniform plane shear flows under various normal stresses, shear strain rates, Young's modulii of the grains and their friction coefficient. We derived an expression for the conductivity tensor as a sum of the contact conductances, which enables instantaneous measurements without simulating the actual heat transfer.

We found that the conductivity tensor is anisotropic and aligns with the direction of the principal stresses (45° with respect to the shear frame), which enables a direct comparison of their eigenvalues. It was also showed that the conductivity i) does not depend on the *inertial number* I which controls the shear state, ii) increases with $\kappa^{1/3}$, κ being the ratio between the normal stress and Young's

modulus, and iii) decreases as grains are more frictional in the range $0.1 \lesssim \mu < 0.8$.

We further found that there is no direct relationship between the conductivity and the stress tensors. This is because the contact heat flux depends on the normal contact force only. On the other hand, the effective conductivity depends on the part of the stresses that carries only the normal contact forces, while it does not depend on that from the tangential contact forces. Along these lines it was noted that the contribution of tangential force to the normal stress is very low (a few percent), compared with that for the tangential stress (about 20%). Finally, we have proposed a semi-empirical scaling law which is robust in its ability to quantitatively relate the conductivity with the contact density, Young's modulus and the part of the stresses relying on the normal forces.

The fundamental insights of this work should provide a useful base for further studies of heat conduction in more realistic granular flows. Features such as the heterogeneities of the conductivity —as they are induced by irregular force chains [10] or from possible heterogeneities in localised heat production, shear rate and stress gradients (*e.g.* due to depth-graded gravity or from spontaneous shear banding)— or non-Hertzian contacts with surface asperities [19,20] should play a significant role on the heat transfer and on the scaling law obtained. For that purpose, actual heat transfer simulations, as proposed in the thermal-DEM [8], should be pivotal.

* * *

Financial support for this research from the Australian Research Council, through grant DP1096958, is gratefully appreciated.

REFERENCES

[1] Barnett W. and Hoopes J., *The Emergence of Pottery: Technology and Innovation in Ancient Societies* (Smithsonian Institution Press) 1995.
[2] Vargas W. and McCarthy J., *Phys. Rev. E*, **76** (2007) 41301.
[3] Divoux T., Gayvallet H. and Géminard J., *Phys. Rev. Lett.*, **101** (2008) 148303.
[4] Chen K., Cole J., Conger C., Draskovic J., Lohr M., Klein K., Scheidemantel T. and Schiffer P., *Nature*, **442** (2006) 257.
[5] Chen K., Harris A., Draskovic J. and Schiffer P., *Granular Matter*, **11** (2009) 237.
[6] Kunii D. and Smith J., *AIChE J.*, **6** (1960) 71.
[7] Batchelor G. and O'Brien R., *Proc. Roy. Soc. London A*, **53** (1977) 313.
[8] Vargas W. and McCarthy J., *AIChE J.*, **47** (2001) 1052.
[9] L. Vargas W. and McCarthy J., *Chem. Eng. Sci.*, **57** (2002) 3119.
[10] Smart A., Umbanhowar P. and Ottino J., *EPL*, **79** (2007) 24002.
[11] Mora P. and Place D., *Geophys. Res. Lett.*, **26** (2001) 123.
[12] Rice J., *J. Geophys. Res.*, **111** (2006) B05311.
[13] Sulem J., Vardoulakis I., Ouffroukh H. and Perdikatsis V., *Soils Found.*, **45** (2005) 97.
[14] Wibberley C. and Shimamoto T., *Nature*, **7051** (2005) 689.
[15] Rempel A. and Rice J., *J. Geophys. Res.*, **111** (2006) B09314.
[16] Otsuki K., Monzawa N. and Nagase T., *J. Geophys. Res.*, **108** (2003) B42192.
[17] Alonso-Marroquín F., Vardoulakis I., Herrmann H., Weatherley D. and Mora P., *Phys. Rev. E*, **74** (2006) 31306.
[18] Hertz H., *J. Reine Angew. Math.*, **92** (1881) 156.
[19] Madhusudana C., *Thermal Contact Conductance* (Springer) 1996.
[20] Bahrami M., Yovanovich M. and Culham J., *Int. J. Heat Mass Transf.*, **49** (2006) 3691.
[21] Kaganer M., *J. Eng. Phys. Thermophys.*, **11** (1966) 19.
[22] Cooper M., Mikic B. and Yovanovich M., *Int. J. Heat Mass Transf.*, **12** (1969) 279.
[23] Feng Y., Han K., Li C. and Owen D., *J. Chem. Phys.*, **227** (2008) 5072.
[24] Christoffersen J., Mehrabadi M. M. and Nemat-Nasser S., *J. Appl. Mech.*, **48** (1981) 339.
[25] Kruyt N. P. and Rothenburg L., *J. Appl. Mech.*, **118** (1996) 706.
[26] Jagota A. and Hui C., *J. Appl. Mech.*, **57** (1990) 789.
[27] Gustafsson S., Karawacki E. and Khan M., *J. Phys. D: Appl. Phys*, **12** (1979) 1411.
[28] Rognon P., Einav I. and Gay C., submitted to *Phys. Rev. E* (2009).
[29] da Cruz F., Emam S., Prochnow M., Roux J.-N. and Chevoir F., *Phys. Rev. E*, **72** (2005) 021309.
[30] Rognon P. G., Roux J.-N., Naaim M. and Chevoir F., *J. Fluid Mech.*, **596** (2008) 21.
[31] GDR MiDi, *Eur. Phys. J. E*, **14** (2004) 341.
[32] Forterre Y. and Pouliquen O., *Annu. Rev. Fluid Mech.*, **40** (2008) 1.
[33] Campbell C., *J. Fluid Mech.*, **539** (2005) 273.
[34] Peyneau P.-E. and Roux J.-N., *Phys. Rev. E*, **78** (2008) 011307.
[35] Majmudar T. and Behringer R., *Nature*, **435** (2005) 1079.